Available online at www.sciencedirect.com
ScienceDirect
ELSEVIER
Journal of Crystal Growth 310 (2008) 2464–2470
JOURNAL OF CRYSTAL GROWTH
www.elsevier.com/locate/jcrysgro

Seeded growth of AlN on SiC substrates and defect characterization

P. Lu[a,b,*], J.H. Edgar[a], C. Cao[a], K. Hohn[a], R. Dalmau[b], R. Schlesser[b], Z. Sitar[b]

[a]*Department of Chemical Engineering, Kansas State University, Manhattan, KS 66506, USA*
[b]*Department of Materials Science and Engineering, North Carolina State University, Raleigh, NC 27695, USA*

Received 11 June 2007; received in revised form 4 October 2007; accepted 2 January 2008
Communicated by M.S. Goorsky
Available online 17 January 2008

Abstract

In this study, seeded sublimation growth of aluminum nitride (AlN) on SiC substrates was investigated. Large diameter (15–20 mm) and thick (1–2 mm) AlN layers were demonstrated on Si-face, 3.5° off-axis 6H-SiC (0 0 0 1). A *c*-axis growth rate of 15–20 μm/h was achieved at 1830 °C, and the surface morphology was highly textured: step features were formed with a single facet on the top of the layer. High-resolution X-ray diffraction (HRXRD), X-ray photoelectron spectroscopy (XPS), and molten KOH/NaOH etching were employed to characterize the AlN layers. The AlN crystals grew highly orientated along the *c*-axis, however, the impurities of Si (3–6 at%) and C (5.9–8 at%) from the SiC changed the lattice constants of AlN and shifted the AlN (0 0 .2) 2θ value from pure AlN toward SiC. All the growth surfaces had Al-polarity and the dislocation density decreased from 10^8 to $10^6\,cm^{-2}$ as the film thickness increased from 30 μm to 2 mm.
© 2008 Elsevier B.V. All rights reserved.

PACS: 81.10.Bk

Keywords: A1. X-ray diffraction; A2. Growth from vapor; A2. Single-crystal growth; B1. Nitrides

1. Introduction

Aluminum nitride (AlN) is a direct wide band gap semiconductor ($E_g = 6.2\,eV$) with high thermal conductivity and high thermal stability. Due to its small mismatches in coefficients of thermal expansion and lattice constants single-crystalline AlN is an ideal substrate for $Al_xGa_{1-x}N$ epitaxial layers, as are needed for high-power UV lasers diodes, UV photodetectors, and blue light-emitting diodes (LEDs). The benefits of AlN substrates were dramatically illustrated by Taniyasu et al. [1], who was able to prepare a silicon-doped AlN epitaxial layer with an extremely high room temperature electron mobility, $400\,cm^2/V\,s$, by using an AlN substrate with a low dislocation density.

Sublimation is the most successful growth method for bulk AlN single crystals, as demonstrated by Slack and McNelly [2,3], Bickermann et al. [4], and others [5–8]. For bulk AlN crystal growth, SiC is a suitable seed since it has a small *a*-lattice constant mismatch (0.96% for 6H-SiC and 1.2% 4H-SiC) [9] with AlN. Large area (up to 100 mm in diameter) and high-quality single-crystalline 4H- and 6H-SiC wafers are commercially available.

There have been many important studies [10–19] of the sublimation growth of AlN on SiC seeds that have established the appropriate temperature range for growth (typically 1750–1900 °C), demonstrated growth rates higher than 10 μm/h, identified the nucleation modes for AlN as a function of process conditions, and grown thick AlN layers (up to several mm thick). Together, this body of research has demonstrated that SiC is feasible as a seed crystal, yet many details concerning the best methods to implement this technology remain to be developed.

The purpose of the present work was to produce thick and large AlN layers by using SiC seeds and extensively

*Corresponding author at: Department of Materials Science and Engineering, North Carolina State University, Raleigh, NC 27695, USA. Tel.: +1 919 515 8804; fax: +1 919 515 3419.
E-mail address: plu@ncsu.edu (P. Lu).

0022-0248/$ - see front matter © 2008 Elsevier B.V. All rights reserved.
doi:10.1016/j.jcrysgro.2008.01.010

characterize the resulting crystals, focusing on the crystal quality, the surface morphology, the impurity concentration and the defect density. This work builds on the author's previous investigation into the initial growth stage of AlN on SiC [20], which established the optimum growth temperature of AlN as 1830–1850 °C, based on 20–30 μm thick single-crystalline AlN films grown on 8° off-axis 4H-SiC and on-axis 6H-SiC. The off-axis-grown film consisted of regular step features on the surface, while the on-axis-grown film contained hexagonal sub-grains of varying sizes.

2. Experimental procedure

The AlN crystals were grown by sublimation in a resistively heated graphite furnace, consisting of a growth chamber, a graphite heating element, graphite foam insulation and a temperature and pressure control system, as illustrated in Ref. [21]. The source material was AlN powder originally containing less than 1 wt% oxygen and 0.06 wt% carbon. Prior to growth, the AlN powers were purified by baking at 1900 °C for 4 h, which reduced the oxygen concentration to less than 0.1 wt%, as measured by gas fusion technique. Si-face, 6H-SiC (0 0 0 1) with a 3.5° mis-orientation toward $(1 1 \bar{2} 0)$ was employed as the substrate. As-received wafers were cut into approximately $2.5 \times 2.5\,\mathrm{cm}^2$ pieces and cleaned in organic solvents in the sequence of trichloroethylene, acetone, and methanol, rinsed with DI water and dried with nitrogen. The substrate was mounted in the top part of the crucible, 3 mm above the surface of the sintered source. The substrate temperature was kept 5–10 °C lower than the source. All samples were grown at a source temperature of 1830 °C. The crystal orientation was examined by high-resolution X-ray diffraction (HRXRD).

The impurities present and their concentrations in the grown crystal were detected and measured by X-ray photoelectron spectroscopy (XPS). Prior to analysis the sample surface was sputtered by Ar ions for 1 h to remove the native oxide layer, which forms when AlN is exposed to ambient air, and then scanned for 20 min. XPS is a surface chemical analysis technique, which reveal the elemental composition of the surface (1–10 nm). In this article, it is assumed that the elemental composition in the bulk crystal is approximately same as the crystal surface. The main point is to qualitatively observe whether the major impurities, Si and C, are present in the AlN layer, rather than a quantified measurement.

To explore the polarity and dislocation density of the grown AlN layers, the samples were etched in a molten KOH/NaOH eutectic alloy (59 wt% KOH/41 wt% NaOH) at 300–310 °C for 5 min. In molten KOH/NaOH, both the N-polarity and the Al-polarity are etched: the N-polarity forms hexagonal hillocks and the Al-polarity forms hexagonal etch pits. The type and the density of dislocations were revealed by the shape and density of the etch pits [22].

3. Results and discussion

3.1. Surface morphology and crystal color

In this paper, two samples (A and B) are discussed. Sample A was continuously grown for a period of 50 h, and sample B was grown in two consecutive 50 h periods. Between the two growths, the crucible was refilled with sintered AlN source. The two samples had similar surface morphologies: the surface consisted of step features, with step widths of 0.3–1 mm and in each case an extended, flat facet formed. The facet of sample A was $9 \times 6\,\mathrm{mm}^2$, as shown in Fig. 1(a). The facet of sample B enlarged from $9 \times 3\,\mathrm{mm}^2$ after the first growth to $9 \times 6\,\mathrm{mm}^2$ after the second growth, as shown in Fig. 1(b) and (c). For both samples, the step terraces were smooth without visible tilted growths or polycrystalline grains, indicating the superior epitaxy, as shown in Fig. 2. However, cracks still appeared on the surface, due to the mismatches in lattice constants and thermal expansion coefficients between AlN and SiC. Samples A and B were approximately 0.9–1 mm and 1.7–2 mm thick, respectively, thus, the *c*-axis growth rate for both was approximately 15–20 μm/h. Sample A exhibited a deep blue color, while sample B had a transparent amber color, implying they contained different impurities or impurity concentrations.

3.2. Crystal quality characterization by high-resolution X-ray diffraction (HRXRD)

The ω-scan double crystal rocking curves (DCRC) characterized the AlN (0 0 .2) peaks in both samples. The full-width at half-maximum (FWHM) of the ω rocking curve (RC) was 1552 and 444 arcsec for samples A and B, illustrated in Fig. 3(a) and (b), respectively. Sample B was of higher crystal quality than sample A. The width and multi-peaked shape of the DCRC scans could be attributed to the presence of cracks in the AlN, bowing of the wafer due to the differential thermal expansion between AlN and SiC, and crystallographic tilt distribution of mosaic blocks. For comparison purpose, the backsides of the two samples (6H-SiC substrate without AlN) were also scanned by DCRC. The (0 0 .6) DCRC of the SiC showed considerable tilt broadening of a similar magnitude as the AlN layer for both samples, indicating the SiC wafer itself had a series of tilted mosaic blocks. The deposited AlN layer may have replicated the mosaicity of the substrate. Thus, the AlN crystal quality may be highly dependent on the quality of the SiC substrate underneath. For both samples the FWHM of (0 0 .2) AlN peaks are of similar magnitude, but slightly smaller than the (0 0 .6) SiC peaks from the back side of the substrate, implying that the grown AlN crystal quality may be as good or better than the SiC substrates. The FWHMs of the (0 0 .2) AlN peaks and the (0 0 .6) SiC are listed in Table 1.

The precise Bragg 2θ angle for the AlN (0 0 .2) peak was 35.97° for both layers as determined by a high-resolution

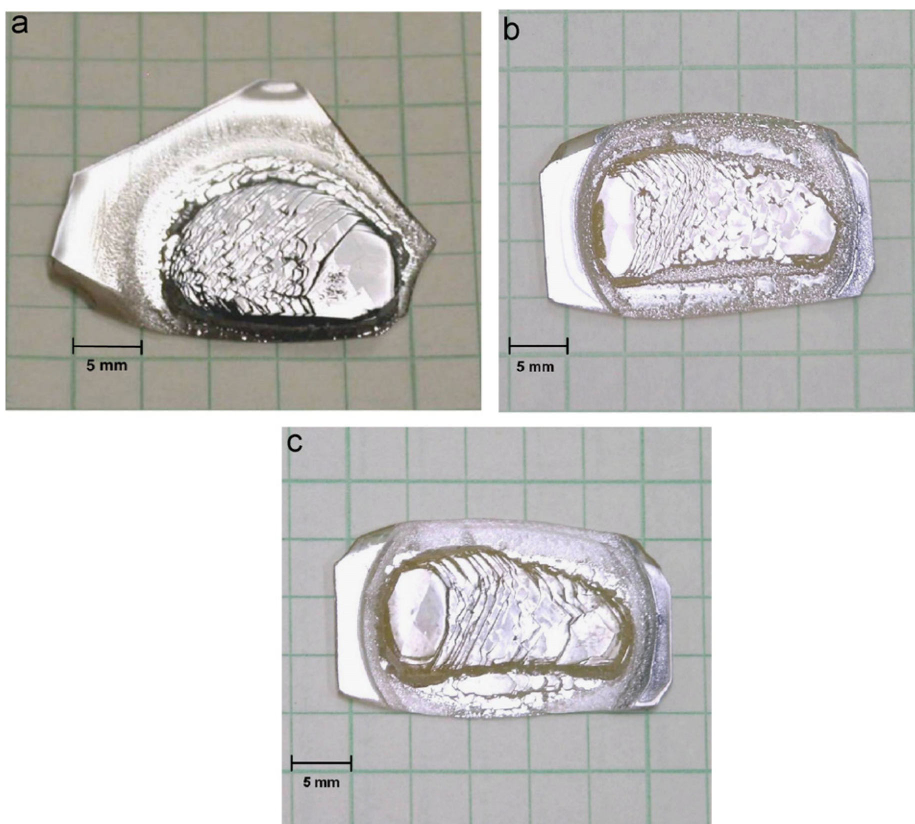

Fig. 1. Images of (a) sample A, grown at 1830 °C for 50 h, (b) sample B, grown at 1830 °C for 50 h, and (c) sample B, grown at 1830 °C for additional 50 h.

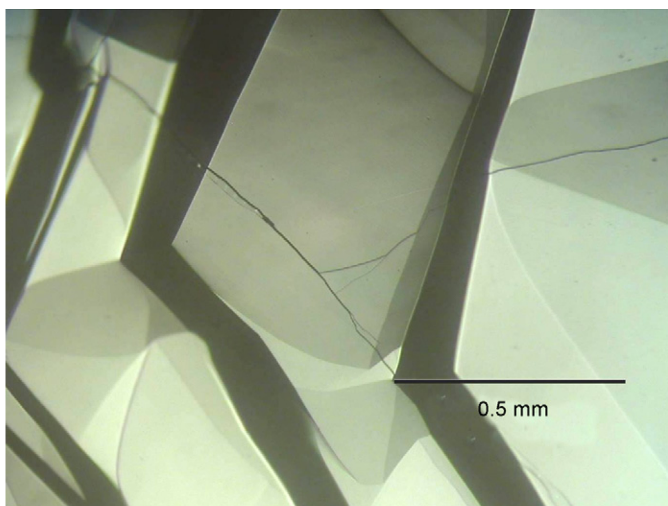

Fig. 2. A micrograph of sample B after the second growth.

triple crystal (0 0 .2) 2θ–ω scan. This value shifted from the powder diffraction file (PDF) database value of AlN (36.04°) toward 6H-SiC (0 0 .6) (35.75°). The shift in the 2θ value was partially caused by the compression of the film, which was generated by the lattice mismatch between the AlN and SiC. In addition, the AlN layer could contain silicon and carbon originating from the decomposition of the SiC seed. This possibility will be discussed below.

3.3. Impurities characterization by X-ray photoelectron spectroscopy (XPS)

The XPS spectra of samples A and B are shown in Fig. 4(a) and (b) and the detected impurities and their atomic concentrations are listed in Table 2. Silicon contamination originated exclusively from the SiC seed, since there was no other silicon source in the furnace. The carbon in the crystals may have originated from the SiC seed and the degradation of graphite components in the furnace. The impurity concentrations in sample A (Si: 6.0 at%, C: 8.1 at%) were higher than in sample B (Si: 3.0 at%, C: 5.9 at%). The differences in the silicon and carbon concentrations are believed to explain the observed color difference between samples A and B.

These two AlN layers were grown under nominally identical conditions; however, the growth conditions were not exactly duplicated due to small changes in the crucible (composition or micro-cracking), the furnace insulation and the heating element. In addition, the quality of the SiC substrate may influence the impurities incorporated in the AlN crystal. A SiC seed with a high micropipe density may generate more volatile silicon and carbon than a seed with low micropipe density, since the decomposition at a micropipe is much faster than in a micropipe-free region.

The surface oxygen concentrations in both samples were 8–9 at%, which were much higher than the bulk values. Because of its strong affinity for oxygen, a native oxide

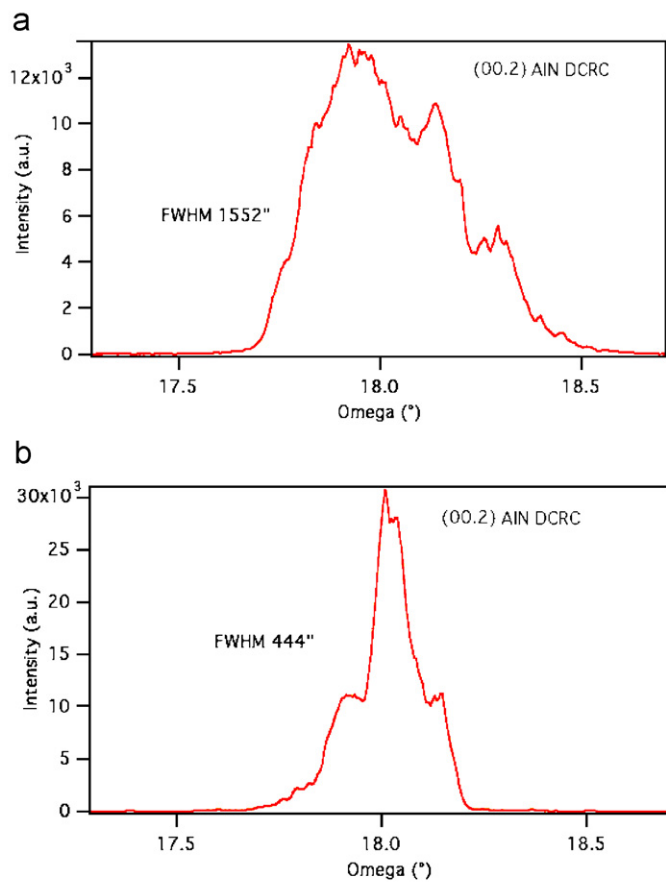

Fig. 3. The ω-scan double crystal rocking curves (DCRC) of the AlN (0 0 .2) peak from (a) sample A, grown at 1830 °C for 50 h, and (b) sample B, grown at 1830 °C for total 100 h.

Table 1
FWHMs of the (0 0 .2) AlN peaks and the (0 0 .6) SiC peaks from the substrates

	Sample A		Sample B	
	AlN (0 0 .2)	6H-SiC (0 0 .6) (substrate)	AlN (0 0 .2)	6H-SiC (0 0 .6) (substrate)
FWHM	1552″	1690″	444″	577″

layer forms on AlN whenever it is exposed to ambient air. Despite sputtering the sample before XPS measurements, oxygen was always detected, suggesting that oxidation occurs even under ultrahigh vacuum conditions. The oxygen concentration measured by XPS always exceeded the concentration of oxygen measured by LECO analysis (a bulk technique) of polycrystalline AlN grown by unseeded growth by two to three orders of magnitude. Since the AlN was grown on SiC substrates from similar source materials under similar conditions, we conclude that the high oxygen concentrations are limited to the surface of the samples.

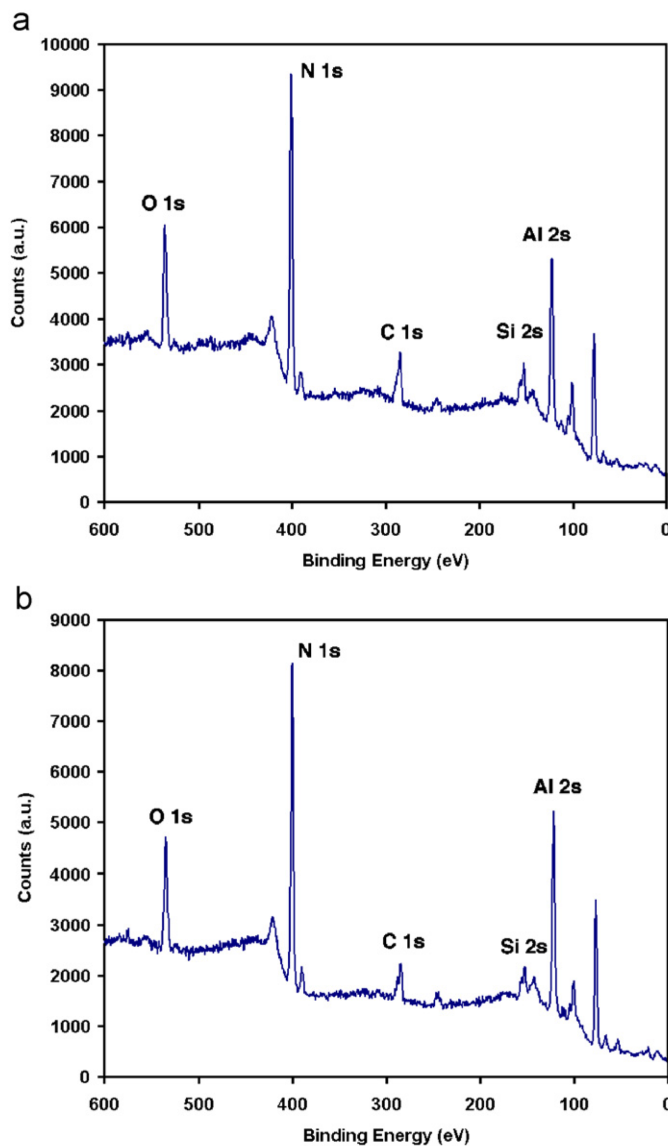

Fig. 4. XPS spectra of (a) sample A and (b) sample B.

Table 2
The detected elements and their atomic concentrations in samples A and B

Elements	At% (sample A)	At% (sample B)
O 1s	9.3	8.5
C 1s	8.1	5.9
Si 2s	6.0	3.0

3.4. Defect characterization by molten KOH/NaOH etching

Molten KOH/NaOH etching revealed only etch pits (no hillocks) on samples A and B, indicating both layers have Al-polar surfaces without N-polar inversion domains. Most of the etch pits are hexagonally shaped, related to threading dislocations. SEM images of the surfaces after etching are shown in Fig. 5 (sample A: (a) and (b); sample B: (c) and (d)). Some etch pits were randomly scattered and

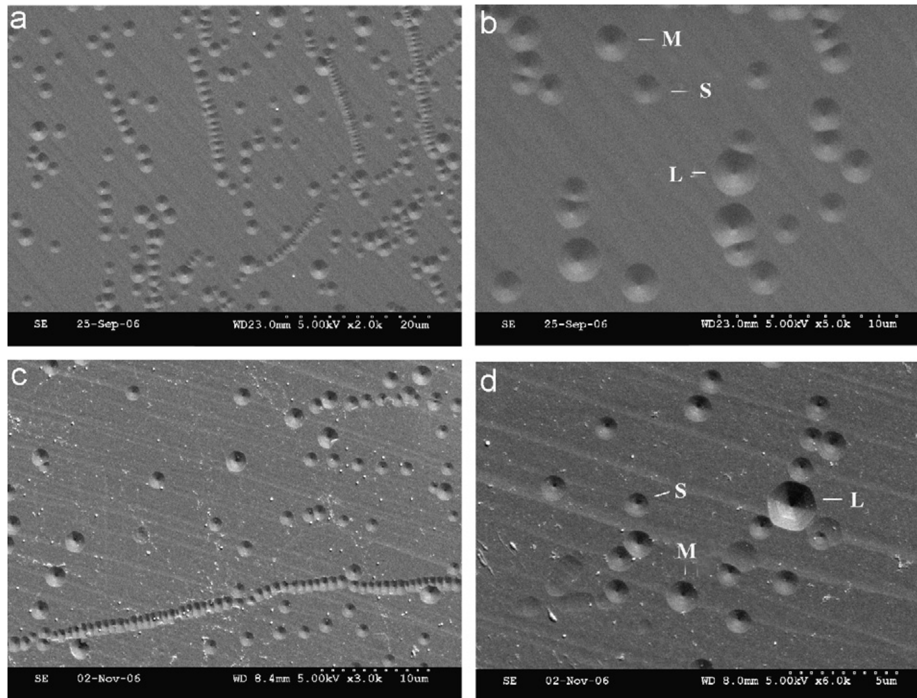

Fig. 5. SEM images of the AlN layers after molten KOH/NaOH etching: (a) sample A, 3 kX, (b) sample A, 5 kX, (c) sample B, 3 kX, and (d) sample B, 6 kX.

some aligned together forming pits arrays, which are related to low angle grain boundaries [23]. The low angle grain boundaries correspond to domain walls, which separate highly perfect crystal grains. The grains might be generated due to different nucleation centers that are slightly misoriented to each other. A higher density of low angle grain boundaries was observed on the thinner sample A (Fig. 5(a)) than on the thicker sample B (Fig. 5(b)), implying sample A contained more crystal grains than sample B. Hence, sample B should be of better crystal quality since the crystal has more uniform orientation with less grains. This result is consistent with the XRD results shown in Fig. 3.

Three etch pit sizes are clearly visible in these figures indicating the presence of three types of dislocations in the films. In Fig. 5(b) and (d), small, medium, and large etch pits are labeled as S, M, and L, respectively. By investigating the molten KOH etching of GaN, Weyher [24] suggested that the smallest etch pits are associated with edge dislocations, the largest pits associated with screw dislocations, and the medium pits associated with mixed edge and screw dislocations. The nitrides, GaN, and AlN, have the hexagonal wurtzite structure. The burgers vectors for edge and screw dislocations are $b = a_{\rm i} = \frac{1}{3}\langle 2\,\bar{1}\,\bar{1}\,0\rangle$ and $b = \langle 0\,0\,0\,1\rangle$, respectively [25,26]. The burgers vectors for mixed dislocations are$b = c + a_{\rm i} = \frac{1}{3}\langle 1\,1\,\bar{2}\,3\rangle$ [25].

The total dislocation densities of sample A (1 mm thick) and sample B (2 mm thick) were approximately 5×10^{6} and $3.5\times10^{6}\,\mathrm{cm}^{-2}$, respectively, as estimated by counting the etch pits in a given area. Combined with the author's previous work [20,27] a graph of dislocation density vs. AlN layer thickness is plotted, Fig. 6. The total dislocation density rapidly decreased from over $10^{8}\,\mathrm{cm}^{-2}$ to less than $10^{7}\,\mathrm{cm}^{-2}$ as the AlN layer thickness increased from 0.03 to 1 mm. However, as the film grew thicker, to 2 mm, the dislocation density tended to reach a saturation value, $3–5\times10^{6}\,\mathrm{cm}^{-2}$. At the initial growth stage (less than 0.05 mm thick), the lattice mismatch between the SiC and AlN, the difference in thermal expansion and numerous nucleation centers created an extremely high-density of dislocations. When dislocations are in close proximity they may react with one another by ''fusion'' or ''annihilation''

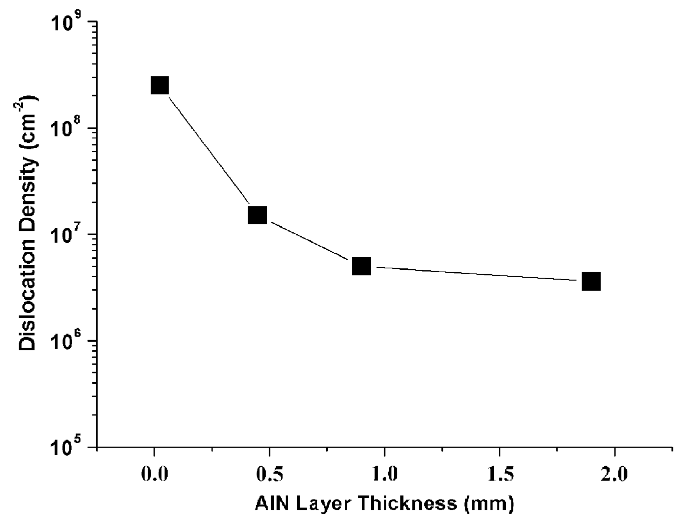

Fig. 6. The relationship of dislocation density and AlN layer thickness.

Table 3
Sub-density percentage of screw, mixed and edge dislocations

AlN layer thickness (mm)	Screw dislocation (%)	Mixed dislocation (%)	Edge dislocation (%)
0.02–0.03	6	21	73
0.25–0.4	7	18	75
1	7	16	77
2	6	11	83

reactions. A fusion reaction occurs when two dislocation become one dislocation with the new Burgers vector $b_3 = b_1 + b_2$ [25]. An annihilation reaction happens when two dislocation lines with opposite Burgers vectors ($b_1 = -b_2$) undergo the reaction $b_1 + b_2 = 0$, removing the dislocation entirely [25].

Table 3 lists the sub-density percentage of screw, mixed, edge dislocations at different thickness. As the total number of dislocation reduced, the percentage of screw dislocation kept constant, the percentage of mixed dislocation steadily dropped and the percentage of the edge dislocation steadily increased. According to the mechanism of the dislocation reduction suggested by Mathis et al. [25], screw dislocations and edge dislocations are parallel to the *c*-axis of the crystal and they cannot move laterally as the crystal growths, therefore they are unlikely to react with the same type of dislocations or react with each other. Mixed dislocations have an inclined line direction relative to *c*-axis, hence they move laterally during growth and interact with other dislocations. The reactions of screw and mixed dislocations produce vertical edge dislocations, and the reactions of edge and mixed dislocations produce vertical screw dislocations. This probably can explain why the percentage of mixed dislocations steadily decreases as the crystal grows. Due to the lack of mixed dislocations the reduction of total dislocation decreases with AlN thickness and will eventually reaches a saturated value, as demonstrated in Fig. 6. This result matches one of the theoretical model developed by Mathis et al. [25].

4. Conclusions

Based on the results presented in this paper, SiC substrates are viable as seed crystals for AlN sublimation growth. The major advantage of this method is the commercial availability of SiC wafers, which provide a large area seed for AlN nucleation and growth, thus enabling the fabrication of large-size AlN crystals, which is very difficult to achieve by self-seeded growth. High-quality SiC wafers are required to (a) reduce defects in the grown AlN, and (b) minimize the decomposition of the SiC substrate.

This approach faces two major challenges: (a) the growth temperature is limited to $<1900\,^{\circ}\mathrm{C}$ in order to slow down the decomposition of the SiC seed, thus resulting in low growth rates of AlN, and (b) contamination of AlN with Si and C is inevitable.

Therefore, an optimized growth procedure only uses SiC as a seed during an initial stage to grow a high quality, large area, and a few mm thick AlN layer, then grind off the SiC substrate to produce a free-standing AlN seed. Subsequently, high temperature ($>2200\,^{\circ}\mathrm{C}$) sublimation growth on this seed will produce a large single-crystal at high growth rates.

Acknowledgments

The support for this work from the National Science Foundation through Grant DMR 0408874 and from Hexatech, Inc. is greatly appreciated.

References

[1] Y. Taniyasu, M. Kasu, T. Makimoto, Appl. Phys. Lett. 89 (2006) 182112.
[2] G.A. Slack, T.F. McNelly, J. Crystal Growth 34 (1976) 263.
[3] G.A. Slack, T.F. McNelly, J. Crystal Growth 42 (1977) 560.
[4] M. Bickermann, B.M. Epelbaum, A. Winnacker, J. Crystal Growth 269 (2004) 432.
[5] E.N. Mokhov, O.V. Avdeev, I.S. Barash, T.Yu. Chemekova, A.D. Roenkov, A.S. Segal, A.A. Wolfson, Yu.N. Makarov, M.G. Ramm, H. Heleva, J. Crystal Growth 281 (2005) 93.
[6] D. Zhuang, Z.G. Herro, R. Schlesser, B. Raghothamachar, M. Dudley, Z. Sitar, J. Electron. Mater. 35 (2006) 1513.
[7] L.J. Schowalter, S.B. Schujman, W. Liu, M. Goorsky, M.C. Wood, J. Grandusky, F. Shahedipour-Sandvik, Phys. Status Solidi A 203 (2006) 1667.
[8] M. Miyanaga, N. Mizuhara, S. Fujiwara, M. Shimazu, H. Nakahata, T. Kawase, J. Crystal Growth 300 (2007) 45.
[9] L. Liu, J.H. Edgar, Mater. Sci. Eng. R37 (2002) 61.
[10] J.H. Edgar, L. Liu, B. Liu, D. Zhuang, J. Chaudhuri, M. Kuball, S. Rajasingam, J. Crystal Growth 246 (2002) 187.
[11] C.M. Balkas, Z. Sitar, T. Zheleva, L. Bergman, R. Nemanich, R.F. Davis, J. Crystal Growth 179 (1997) 363.
[12] W.L. Sarney, L. Salamanca-Riba, T. Hossain, P. Zhou, H.N. Jayatirtha, H.H. Kang, R.D. Vispute, M. Spencer, K.A. Jones, MRS Internet J. Nitride Semicond. Res. 5S1 (2000) W5.5.
[13] L. Liu, B. Liu, Y. Shi, J.H. Edgar, MRS Internet J. Nitride Semicond. Res. 6 (2001) 7.
[14] Y. Shi, Z.Y. Xie, L. Liu, B. Liu, J.H. Edgar, M. Kuball, J. Crystal Growth 233 (2001) 177.
[15] Y. Shi, B. Liu, L. Liu, J.H. Edgar, H.M. Meyer III, E.A. Payzant, L.R. Walker, N.D. Evans, J.G. Swadener, J. Chaudhuri, Phys. Status Solidi A 188 (2001) 757.
[16] B.M. Epelbaum, M. Bickermann, A. Winnacker, Mater. Sci. Forum 983 (2003) 433.
[17] R. Dalmau, R. Schlesser, B.J. Rodriguez, R.J. Nemanich, Z. Sitar, J. Crystal Growth 281 (2005) 68.
[18] S. Wang, B. Raghothamachar, M. Dudley, A.G. Timmerman, Mater. Res. Soc. Symp. Proc. 892 (2006) 775.
[19] K. Balakrishnan, M. Banno, K. Nakano, G. Narita, N. Tsuchiya, M. Imura, M. Iwaya, S. Kamiyama, K. Shimono, T. Noro, T. Takagi, H. Amano, I. Akasski, Mater. Res. Soc. Symp. Proc. 831 (2005) 607.
[20] P. Lu, J.H. Edgar, R.G. Lee, J. Chaudhuri, J. Crystal Growth 300 (2007) 336.

[21] B. Liu, J.H. Edgar, B. Raghothamachar, M. Dudley, J.Y. Lin, H.X. Jiang, A. Sarua, M. Kuball, Mater. Sci. Eng. B 117 (2005) 99.
[22] D. Zhuang, J.H. Edgar, B. Strojek, J. Chaudhuri, Z. Rek, J. Crystal Growth 262 (2004) 89.
[23] D. Hull, D.J. Bacon, Introduction to Dislocations, third ed., Butterworth-Heinemann, Oxford, 1984, pp. 13–16.
[24] J.L. Weyher, Superlatt. Microstruct. 40 (2006) 279.
[25] S.K. Mathis, A.E. Romanov, L.F. Chen, G.E. Beltz, W. Pompe, J.S. Speck, J. Crystal Growth 231 (2001) 371.
[26] X.H. Wu, L.M. Brown, D. Kapolnek, S. Keller, B. Keller, S.P. DenBaars, J.S. Speck, J. Appl. Phys. 80 (1996) 3228.
[27] P. Lu, J.H. Edgar, C. Cao, K. Hohn, R. Dalmau, R. Schlesser, Z. Sitar, Mater. Res. Soc. Symp. Proc. 955 (2007).